# Diffuse Acoustic Field Produced in Reverberant Rooms: A Boundary Diffuse Field Index

Jean-Daniel Chazot, Olivier Robin, Jean-Louis Guyader, Noureddine Atalla

# Diffuse Acoustic Field Produced in Reverberant Rooms: A Boundary Diffuse Field Index

Jean-Daniel Chazot[1)], Olivier Robin[2)] Jean-Louis Guyader[3)], Noureddine Atalla[2)]

[1)] Sorbonne universités, Université de technologie de Compiègne, CNRS, Laboratoire Roberval UMR 7337, 60203 Compiègne Cedex, France. jean-daniel.chazot@utc.fr

[2)] Groupe d'Acoustique de l'Université de Sherbrooke, Université de Sherbrooke, 2500 boulevard de l'université, Sherbrooke (Québec) J1K 2R1, Canada

[3)] Laboratoire Vibrations Acoustique de l'INSA de Lyon, 25 bis, avenue Jean Capelle, 69621 Villeurbanne Cedex, France

**Summary**

An as diffuse as possible acoustic field is pursued when performing measurements that make use of a reverberant room. The diffusivity descriptors that are commonly used to qualify the actual sound field in such a room are calculated in the room volume, away from boundaries. This is somewhat contradictory with the fact that for sound insulation and sound absorption measurements as examples, specimens are placed at room boundaries either a wall or the floor. This work presents a characterization of the sound pressure field at the boundaries of a reverberant room in order to evaluate the diffusivity of the excitation at these specific locations. A boundary diffuse field index is proposed, numerically evaluated and then tested in two reverberant chambers in steady state conditions. It is shown that this index allows evaluating the boundary diffusivity in a given reverberant room according to its geometry and other relevant parameters, such as the sound source location or the presence of sound diffusers.

**PACS no. 43.55.Br, 43.55.Cs, 43.55.Nd**

## 1. Introduction

A reverberant room is used in several standardized measurements, such as the sound absorption of materials [1, 2], the sound power of noise sources [3] or the sound insulation of partitions [4, 5, 6, 7]. A common assumption to all these measurements is that the sound field in the room is perfectly diffuse. Following Sabine's theory and formalism [8], this hypothesis was shown to be satisfied above the cut-off frequency of the room [9] when room modes separation becomes small so that modes begin to overlap. Simple relationships can be then established as between the sound decay rate in the room and the room volume and an equivalent sound absorption area, or between the spatially averaged mean square pressure and the sound intensity in the room. Improvements to Sabine's theory to better take into account room geometry, damping distribution or variation of the absorption coefficient with incidence angle were proposed by Eyring [10, 11], or Millington [12], but a uniform sound field was still assumed above the cut-off frequency.

From both theoretical and experimental views, completely diffuse conditions are impossible to reach. Ensuring and qualifying effective sound diffusion in the room becomes of crucial importance, since the previously mentioned relationships will be biased if the actual conditions diverge from the perfect diffuse field assumption. Standards [4, 5, 1, 3, 2, 6, 7] thus include several recommendations and tests to qualify the performance of a given reverberant room. A considerable number of special devices was proposed and tested to improve diffusivity such as hanging, rotating, corner or boundary diffusers [13, 14, 15, 16, 17, 18]. Nevertheless, several studies [19, 20, 21, 22, 23, 24] have shown the variability of transmission loss measurements between different laboratories at low frequency, and also surprisingly at high frequency where a diffuse field independent of excitation conditions would be expected as well as a good inter-laboratory reproducibility of measurements. Similar issues were reported for sound absorption coefficient measurements [13, 25, 26, 27, 28, 29] and studied by simulations using a ray tracing method [30, 31], with important variations of sound absorption coefficients according to excitation conditions such as room absorption, room shape and the number of diffusers in the room.

Several definitions of a diffuse acoustic field [32] and corresponding diffusivity indicators have been proposed. A usual definition is that uniform sound pressure at all locations in the reverberant room should be obtained (the sound pressure level does not vary with receiver position). Another definition is that the propagation of sound in

any direction is equiprobable and phase relation between sound waves is random so that they are uncorrelated. Finally, an alternate formulation is that at any position in the room, sound energy is incident from all directions with equal intensities.

In practice a first method to verify the diffuseness relies on the measurement of sound pressure at different locations in a reverberant room, in order to check the spatial uniformity assumption (which is proposed in standards test procedures, see Annex A2 in [7] for example). Another possibility is to verify that all directions of propagation are equiprobable, and the use of a rotating directional microphone [33] and an Ambisonic microphone [34] was tested. A microphone array measurement system was also proposed by Gover [35], where directional and spatial variations of sound fields were examined.

Among these methods, one of the most studied ways to verify the diffuseness of the sound field has been the estimation of the cross correlation function or of its Fourier transform, the cross-spectral density function. The cross-correlation function was theoretically found to follow a *sinc* function behavior for a perfect diffuse acoustic field [36, 37], which writes $\sin(k_0\mathbf{x})/k_0\mathbf{x}$ where $k_0$ is the acoustic wavenumber and $\mathbf{x}$ is the vector distance between two points (statistical properties of such a reverberant sound field are for example given in [38, 39]). Experimental estimations of the cross-correlation function were mainly conducted using two microphones [36, 13, 40, 41] (usually with one still microphone and a mobile one, so that $\mathbf{x}$ can be varied) or using microphone arrays [42, 43], and good agreement with theoretical predictions was generally obtained. However, the satisfaction of the *sinc* function criterion has been proven to be a necessary, but not a sufficient condition to verify the effective realization of a diffuse sound field [44]. This function has nevertheless been useful to model a diffuse excitation when the exact excitation distribution is unknown [45]. It was also used for defining the target pressure field when synthetizing a diffuse field on a surface with an array of loudspeakers [46, 47]. In Nélisse and Nicolas [48], the diffuse field in reverberant rooms has been characterized with the correlation function and spatial uniformity both evaluated with a classical modal approach, and a minimum of 20-30 modes in the considered frequency bandwidth was recommended to reach adequate diffuseness following the two evaluated descriptors. Finally, the measurement of coherence functions instead of correlation functions was also proposed, using an intensity probe which allows calculating the coherence between sound pressure or particle velocity components [49], or using microphones only [50].

A common characteristic to these indicators is that they always target verifying diffusion in the volume of the room but never at boundaries where diffusivity is usually restricted to a limit incidence angle. Besides, due to intensification zones at boundaries [51] the diffuse field distribution at room boundaries can not be assimilated to the distribution inside the volume. Also, all these indicators provide a qualitative information concerning a possible degree of diffusion but no quantitative and practical information to help taking into account any deviation of the actual pressure field from the theoretical one. Only recently, a laboratory correction was proposed to consider non-uniform intensity distributions over angles of incidence for transmission loss measurements [52].

In the present work, a classical modal expansion is used to study the sound field distribution and its diffusivity in a rectangular room, particularly at boundaries. Modal decoupling is used as a simplification since considered damping loss coefficients are small [53]. Sabine's assumptions for a diffuse sound field are evaluated, and a free wave model is also used to simply illustrate important facts at boundaries since both eigenmodes and free-wave models were found consistent to describe diffuse acoustic fields [54].

A new descriptor adapted to characterize the sound field diffusivity at boundaries is defined and called Boundary Diffuse Field Index (BDFI). Its averaged value over a measurement surface can be related to a limit incidence angle or to the presence of correlated plane waves, and its standard deviation can be related to the spatial sound distribution over a surface. This descriptor is first evaluated with the classical modal method. Then measurements of the BDFI in two reverberant chambers are presented in steady state conditions.

## 2. Acoustic Field Model

Several kinds of model can be used to describe the sound pressure field inside a room. For small rooms, a modal expansion is usually employed, while wave models are generally preferred for large rooms with large reverberation times. In this section, both models are presented and used to characterize a rectangular reverberant room of dimensions $L_x \times L_y \times L_z$, which is illustrated in Figure 1 with coordinate axes and respective positions of an acoustic source and a window (which utility will be precised later).

The different configurations that will be used for calculations and measurements are detailed in Table I, following the notations given in Figure 1. On one side, configurations C concern simulated reverberant rooms, in which were varied source position (C1a to C1d) or window position (C1a, C1e and C1f) while the dimensions of the room were kept constant. Cases C2 and C3 were based on fixed relative source and window positions, while room dimensions were now varied. On the other side, configurations E and G concern tests performed in two real reverberant rooms. Window positions were fixed for both experimental cases, while source position was varied. Note that room G was equipped with diffusers that were uninstalled once in the case of configuration G1, while room E had no diffusers. It is also precised that window positions were mainly chosen so as to be centered on one wall of the room, and source positions were arbitrarily determined so as to span very different cases, since in laboratory experiments, the position of a test object is usually unchanged (especially for

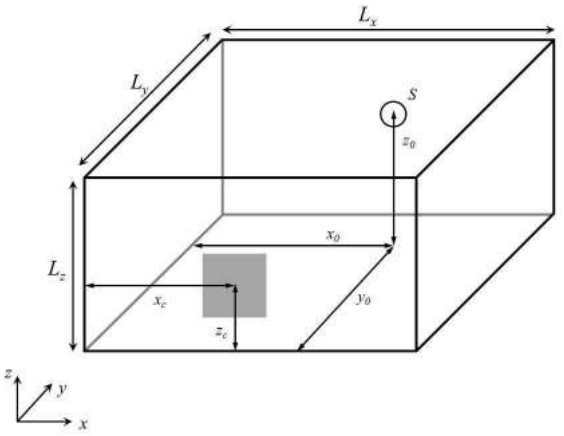


Figure 1. A schematic of the studied rectangular reverberant room of dimensions $L_x \times L_y \times L_z$ - the source location is denoted by $S$, and the grey area denotes a measurement window located in a wall at $y = 0$.

sound insulation tests for which the opening between two rooms can be hardly varied) but the source position can be easily modified if ever needed. Finally, the discretization values $N_x$ and $N_y$ given in the last column of Table I correspond to the number of considered patches in the $x$ and $y$ directions for simulations, and then the number of microphones positions for measurements.

### 2.1. Classical Modal Expansion

The reverberant and boundary sound pressures in a given reverberant room are calculated with the classical modal expansion of the room pressure (time dependence $e^{j\omega t}$ is omitted for sake of simplicity)

$$P(x, y, z) = \sum_{p,q,r} A_{pqr}\psi_{pqr}(x, y, z), \tag{1}$$

where $p, q, r$ are positive integers. In this expansion, a $pqr$ mode is defined by an amplitude $A_{pqr}$, a norm $N_{pqr}$, a wave number $k_{pqr}$, and a mode shape $\psi_{pqr}$

$$A_{pqr} = \frac{\int_{V_r} \psi_{pqr}(x, y, z) S(x, y, z)\, \mathrm{d}V}{\left(k^{*2} - k_{pqr}^2\right) N_{pqr}}, \tag{2}$$

$$N_{pqr} = \int_{V_r} \psi_{pqr}^2(x, y, z)\, \mathrm{d}V, \tag{3}$$

with $V_r$ the room volume, $S(x, y, z)$ the source distribution, and $k^*$ the complex acoustic wave number that takes into account acoustic damping $\eta_r$ such as $k^* = \omega/(c\sqrt{(1 + j\eta_r)})$. Acoustic damping can also be related to the room reverberation time $T_r$ thanks to the relation $\eta_r = 2.2/(f.Tr)$, with $f$ the frequency. The cut-off frequency $f_c$, or Schroeder frequency [9], of the room is finally calculated following $f_c = 2000\sqrt{(T_r/V_r)}$.

For a rectangular room with rigid boundary conditions and excited by an omnidirectional point source located at $x_0$, $y_0$, $z_0$ (see Figure 1), the mode shape, the source distribution, and the modal wavenumber respectively write

$$\psi_{pqr}(x, y, z) = \cos\left(\frac{p\pi}{L_x}x\right)\cos\left(\frac{q\pi}{L_y}y\right)\cos\left(\frac{r\pi}{L_z}z\right), \tag{4}$$

$$S(x, y, z) = S_0\delta(x - x_0)\delta(y - y_0)\delta(z - z_0), \tag{5}$$

$$k_{pqr} = \sqrt{\left(\frac{p\pi}{L_x}\right)^2 + \left(\frac{q\pi}{L_y}\right)^2 + \left(\frac{r\pi}{L_z}\right)^2}. \tag{6}$$

The spatially-averaged square room pressure $P_r^2$, related to the source power and the room absorption, is obtained by averaging the squared pressure over the room volume

$$P_r^2 = \frac{\sum\limits_{p,q,r} \int_{V_r} |A_{pqr}^2| \left(\psi_{pqr}(x, y, z)\right)^2 \mathrm{d}V}{V_r}. \tag{7}$$

Finally, the local boundary pressure (at $y = 0$ for example), also called blocked pressure $P_b$, is obtained by averaging the pressure on a small boundary surface $S_i$.

$$\langle P_b \rangle_i = \frac{\int_{Si} \left( \sum\limits_{p,q,r} A_{pqr}\psi_{pqr}(x, 0, z) \right) \mathrm{d}x\, \mathrm{d}z}{S_i}. \tag{8}$$

This local pressure can be used as an applied external surface force in a finite element model or in a patch transfer function model for estimating the transmission loss of double panels, as in [55, 56]. Contrarily to the spatially-averaged square room pressure, this local boundary pressure is not mean squared over the surface $S_i$ to keep the physical meaning and the phase information of this deterministic pressure. However only the numerical blocked pressures are averaged over a patch surface to get a consistent value of the local pressure instead of a pressure value on a single point. In the measurements the local blocked pressures are just averaged over the microphones diaphragm surface.

A first comparison between a local boundary pressure and the spatially-averaged square room pressure, respectively, is presented in Figures 2a,b for room configuration C1a (see Table I). The spatially-averaged square room pressure dynamic range decreases with increasing modal density (Figure 2a), while the blocked pressure exhibits a very high dynamic range (Figure 2b). This dynamic range difference with blocked pressures is related to the different integration domains. Indeed, blocked pressures are just averaged over small patch surfaces, whereas the room pressure is averaged over the room volume.

Figures 2c-f compare calculated blocked pressure distributions for two window positions (C1a and C1e) and averaged on two third octave bands (250 Hz and 1600 Hz center frequencies). As expected, higher homogeneity is obtained when frequency increases. For the 250 Hz third octave band (Figures 2c,d), acoustic wavelengths are indeed too large to get a diffuse field. However, even if the acoustic field is more homogeneous at 1600 Hz (Figures 2e,f) one can still observe some pressure patterns with sound pressure level differences around 3 dB.

Table I. Details of tested configurations (SI units).

| Name | Room Size $L_x, L_y, L_z$ | Cut off frequency $f_c$ | Source $x_0, y_0, z_0$ | Window center $x_c, z_c$ | Window size $l_x, l_z$ | Discretization $N_x, N_z$ |
|---|---|---|---|---|---|---|
| **Simulation cases** | | | | | | |
| C1a | 7, 4, 3 | 529 Hz | 1, 3, 1.75 | 3.5, 1.5 | 0.75, 0.75 | 20, 20 |
| C1b | 7, 4, 3 | 529 Hz | 2, 3.5, 1.75 | 3.5, 1.5 | 0.75, 0.75 | 20, 20 |
| C1c | 7, 4, 3 | 529 Hz | 1, 1, 1.75 | 3.5, 1.5 | 0.75, 0.75 | 20, 20 |
| C1d | 7, 4, 3 | 529 Hz | 2, 0.5, 1.75 | 3.5, 1.5 | 0.75, 0.75 | 20, 20 |
| C1e | 7, 4, 3 | 529 Hz | 1, 3, 1.75 | 1.75, 1.5 | 0.75, 0.75 | 20, 20 |
| C1f | 7, 4, 3 | 529 Hz | 1, 3, 1.75 | 5.25, 1.5 | 0.75, 0.75 | 20, 20 |
| C2 | 4, 7, 3 | 529 Hz | 1, 6, 1.75 | 2, 1.5 | 0.75, 0.75 | 20, 20 |
| C3 | 6, 5, 2.5 | 545 Hz | 1, 4, 1.75 | 3, 1.25 | 0.75, 0.75 | 20, 20 |
| **Experimental cases** | | | | | | |
| E1 | 5.3, 2.7, 3 | 668 Hz | 4.85, 2.25, 1.7 | 2.37, 1.35 | 0.97, 0.67 | 30, 20 |
| E2 | 5.3, 2.7, 3 | 668 Hz | 4.85, 0.35, 1.7 | 2.37, 1.35 | 0.97, 0.67 | 30, 20 |
| E3 | 5.3, 2.7, 3 | 668 Hz | 4.2, 0.9, 1.7 | 2.37, 1.35 | 0.97, 0.67 | 30, 20 |
| E4 | 5.3, 2.7, 3 | 668 Hz | 4.6, 1.4, 1.7 | 2.37, 1.35 | 0.97, 0.67 | 30, 20 |
| G1 | 7.5, 6.2, 3 | 410 Hz | 6.6, 5.3, 1.5 | 3.75, 1 | 0.8, 0.8 | 9, 9 |
| G2 | 7.5, 6.2, 3 | 410 Hz | 3.75, 3.1, 1.5 | 3.75, 1 | 0.8, 0.8 | 9, 9 |

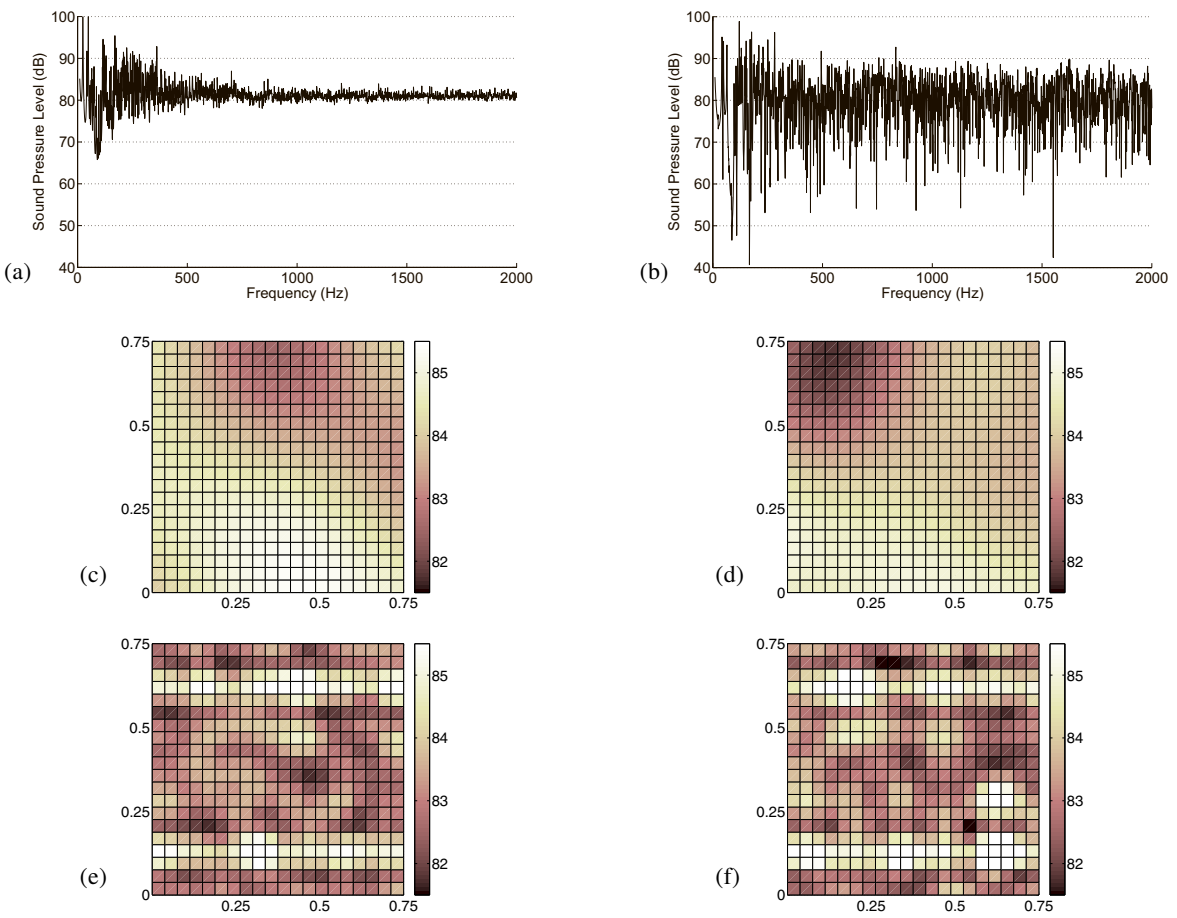


Figure 2. (a) Room pressure using Equation (7) for room configuration C1a. (b) Calculated blocked pressure using Equation (8) for room configuration C1a. (c) Window location C1a - 250 Hz third octave. (d) Window location C1e - 250 Hz third octave. (e) Window location C1a - 1600 Hz third octave. (f) Window location C1e - 1600 Hz third octave. For all figures, source magnitude $S_0 = 2$ Pa.

This shows that a link between uniformity and diffusivity is not always straightforward, even above the cut off frequency of the room (here 529 Hz) when the number of modes is theoretically sufficient to get a uniform diffuse field. In the following some elements are provided in order to evaluate diffusivity and uniformity of boundary pressure fields.

### 2.2. Free Wave model

A perfect diffuse field is assumed according to Sabine's theory with an isotropic sound field consisting of incident uncorrelated plane waves coming from all directions. The square reverberant pressure $P_r^2$ is therefore related to incident plane waves with similar amplitude $P_i$ as

$$P_r^2 = \int_\Omega P_i^2 \, \mathrm{d}\Omega = \int_0^{2\pi} \int_0^{\pi} P_i^2 sin(\theta) \, \mathrm{d}\theta \, \mathrm{d}\varphi = 4\pi P_i^2. \quad (9)$$

Local square boundary pressure $P_b^2$ is obtained by limiting the solid angle to a half space, and by taking into account reflected waves under the assumption of perfectly rigid walls,

$$\begin{aligned} P_b^2 &= \int_{\Omega/2} (2P_i)^2 \mathrm{d}\Omega = \int_0^{\pi} \int_0^{\pi} 4P_i^2 sin(\theta) \, \mathrm{d}\theta \, \mathrm{d}\varphi \\ &= 8\pi P_i^2 = 2P_r^2. \end{aligned} \quad (10)$$

This equation illustrates the classical sound pressure increase of 3dB in a diffuse field at boundaries (*i.e.* pressure doubling). It is also possible to use a limit incidence angle to suppress grazing waves. Figure 3 presents the variations of the ratio $P_b^2/P_r^2$ according to this limit incidence angle. In simulations, a limit angle value of 78 deg ('field incidence') is commonly used. In this case a value of 1.6 is obtained for the $P_b^2/P_r^2$ ratio.

## 3. Boundary Diffuse Field Index

The limit incident angle used to fit a model with an experiment, even at high frequency and for large rooms, proves that the isotropy condition of the diffuse field near boundaries is not fulfilled. This section presents a way to evaluate this diffusivity according to Sabine's description (isotropic field and uncorrelated waves).

A perfect diffuse field according to Sabine's assumptions yields a ratio of 2 between the boundary pressure and the room pressure (see Equation 10). From the classical modal expansion, it is possible to evaluate this ratio locally by using the spatially-averaged squared room pressure (Equation 7) and the local squared boundary pressure over a patch surface (from Equation 8). This ratio can be seen as an index of diffusivity at boundaries, and is therefore called the Boundary Diffuse Field Index,

$$\mathrm{BDFI} = \frac{\left| \left\langle P_b \right\rangle_i \right|^2}{\mathrm{P}_r^2}. \quad (11)$$

This index can be estimated with the classical modal expansion or measured directly with microphones inside the reverberant room. Note however that the local value of the Boundary Diffuse Field Index is not statistically pertinent and should not be compared directly to Equation (10). It is indeed important to evaluate its mean value and its standard deviation over a large surface corresponding to a given measurement window (as an example, the surface of a panel for which the transmission loss is to be measured) to evaluate the diffusivity of the sound field on this area

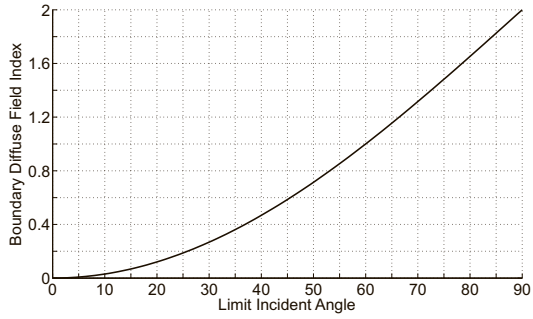


Figure 3. Influence of the incidence angle over the ratio $P_b^2/P_r^2$.

$$\overline{\mathrm{BDFI}} = \frac{\sum_{i=1}^{N} \left| \left\langle P_b \right\rangle_i \right|^2}{N.\mathrm{P}_r^2}, \quad (12)$$

$$\sigma = \sqrt{\frac{1}{N} \sum_{i=1}^{N} \left( \frac{\left| \left\langle P_b \right\rangle_i \right|^2}{\mathrm{P}_r^2} - \overline{\mathrm{BDFI}} \right)^2}. \quad (13)$$

Only this averaged BDFI is significant and can be compared with the ratio obtained in Equation (10). Here the room pressure is assumed to be spatially uniform. In practice, several fixed microphones or a moving microphone are generally used to measure the mean sound pressure in the room.

An example of Boundary Diffuse Field Index averaged over a large surface with 400 patches (that is $N_x \times N_y$ patches for simulation cases in Table I) is presented in the upper part of Figure 4. Large variations over frequency are visible especially in the low frequency domain where obtained values greatly differ from the theoretical value obtained with the plane waves summation in Equation (10). This large dynamic range is surprising since a significant surface is employed, but the variations tend to decrease with increasing frequency and move towards a mean value of approximately 1.75 which is in good agreement with the free wave model when a limit angle of approximately 85 deg is used. Note that this limit angle is usually used as a simple way to tune a numerical model but does not explain all the differences that can be observed between a numerical model and the measurements. These differences can also be due to finite size effects that modify the radiation impedance, possible structural coupling with the acoustic field, and even niche effects concerning transmission loss measurements.

Frequency averaging over third octave bands was used to derive a more representative index. An example of fre-

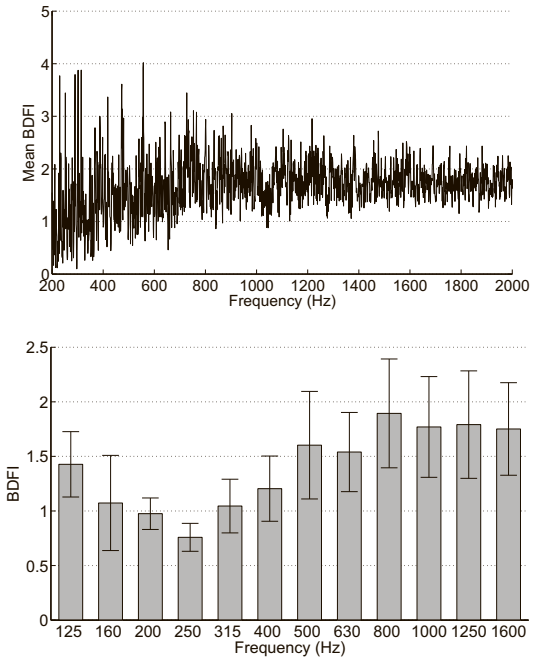


Figure 4. Configuration C1a : (Upper) Calculated mean BDFI - (Lower) Frequency averaged mean BDFIs and standard deviations (indicated by error bars).

quency averaged Boundary Diffuse Field Indices calculated over a large surface with 400 patches is presented in the lower part of Figure 4, with mean values and standard deviations presented on third octave bands from 125 to 1600 Hz. Averaged BDFIs tend to values of 1.75 with a standard deviation of 0.35. Thereby, the perfect diffusivity assumed with the plane wave summation is globally not reached. A BDFI greater than 2 is related to correlated waves, while a BDFI lower than 2 is related to a maximum incidence angle lower than the 90 deg ideal value. In fact the two phenomenons can interact in opposite ways and cannot be distinguished. Comparison with the theoretical value of a perfect diffuse field only illustrates the main phenomenon. In practice, at low frequency the BDFI can exhibit very high or very low values since the modal behaviour of the room is dominant. However transmission loss and absorption measurements are still made in these low frequencies even if the diffuse field asumption is not verified anymore. This is one of the reasons that explain the problems of repeatability and reproducibility often encountered in such measurements. In these cases it would be interesting to normalize the excitation conditions to get a BDFI around 2 at low frequency to potentially improve the repeatability and reproducibility. On the other hand, at high frequency a diffuse sound field is expected. Typically, the Schroeder cut off frequency (here 529 Hz) is usually taken as the limit between the modal behaviour and the diffuse field. In this later case, values lower than 2 could be related to a limit incidence angle in experiments ('field incidence', with a limit incidence angle of 78 deg). Using this previous value in Equation (10), the theoretical BDFI equals 1.6 (see Figure 3), which is close to the high frequency limit obtained with the modal analysis. Again, the BDFI could help taking into account deviations between theory and practice now above the Schroeder frequency.

Standard deviations presented in the lower part of Figure 4 can also be used to evaluate the homogeneity of the boundary sound field. At low frequency the BDFI distribution is quite smooth due to large wavelengths. This leads to low standard deviations of the BDFIs. At medium frequency, at the interface between the modal behavior and the diffuse field, the wavelengths are smaller but the boundary pressure field is not yet uniform. This is observed by the large standard deviations of the BDFIs. At high frequency, the boundary diffuse field should be more uniform and characterized by BDFIs with lower standard deviations. This is not well observed in the lower part of Figure 4. We can then conclude that this boundary pressure field is not perfectly diffuse.

It is therefore important to distinguish the sound field uniformity, and its diffusivity that is related to properties of isotropy. For instance, adding supplementary sound absorption will improve the sound field uniformity but not necessarily its diffusivity since the number of wave reflections decreases with increasing room absorption.

## 4. Parametric study

The classical modal expansion is now used to evaluate the influence of excitation conditions on boundary diffusivity. In this study the patch size is limited by the criterion used in finite element models to get the wavelength patterns, ie. one quarter of an acoustic wavelength.

Figure 5 schematically describes the configurations that are now numerically studied (see details in Table I). Mean BDFI values and their standard deviations obtained with the four source positions C1a-C1b-C1c-C1d are presented in Figure 6a and show that the boundary pressure field diffusivity is very sensitive to the source location at low frequency. This is due to the modal behavior of the room. On the contrary, above 500 Hz the obtained mean BDFIs tend to similar values around 1.8 and confirm a possible lack of grazing waves that can be taken into account with the limit incidence angle. On one hand, the greater direct field contribution for the C1d source position tends to increase the mean BDFI at high frequency. On the other hand, the amplifying effect given by a source near a wall, i.e. C1b, leads also to an increase of the mean BDFI at low frequency. Spatial standard deviations are presented in Figure 6b. Their values do not necessarily decrease above the cut-off frequency, and are also very dependant on the source location at low frequency.

The case of three different window positions (configurations C1a-C1e-C1f) has been tested, and corresponding results are given in Figure 7. Large BDFIs differences related to the room modal behavior are still visible at low frequency. The mean BDFIs tend to a value of 1.8 at high frequency, while the standard deviations values tend to 0.5. Finally, the higher direct field contribution on window C1e is also visible with higher BDFI values.

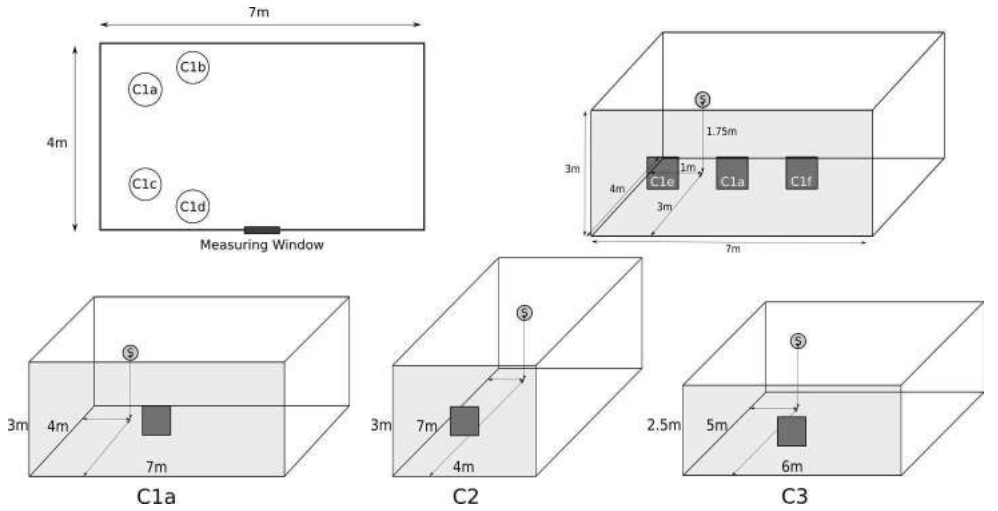


Figure 5. Schematics of tested configurations, detailed in Table I.

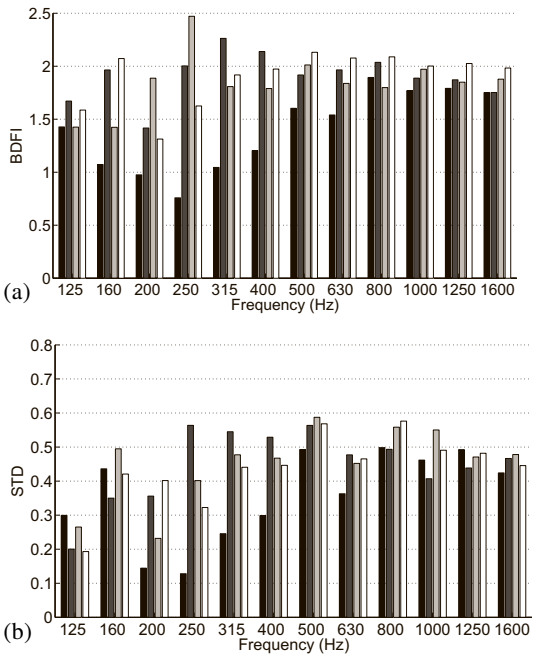


Figure 6. Source position influence on the mean values and Standard deviations of the calculated BDFIs over 400 patches - Configs. ■ C1a ■ C1b ■ C1c □ C1d.

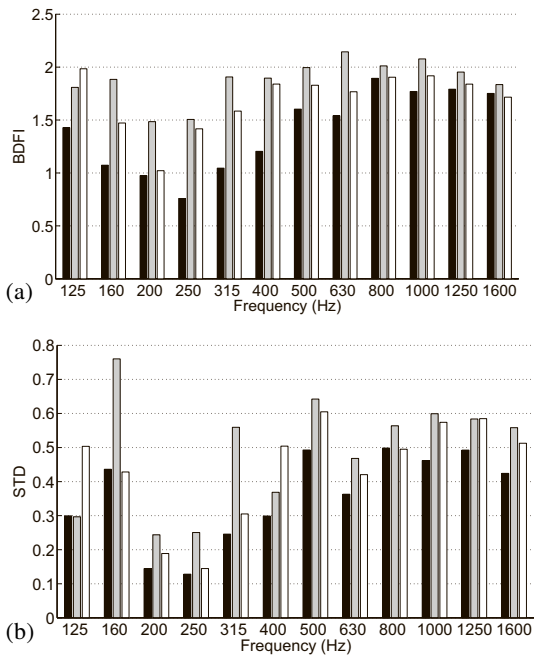


Figure 7. Window position influence on the mean values and standard deviations of the calculated BDFIs over 400 patches - Configs. ■ C1a ■ C1e □ C1f

The effect of different room configurations is finally presented in Figure 8, for C1a-C2-C3 room configurations. The mean BDFIs tend to a lower value of 1.6 at high frequency. This corresponds to an acoustic field limited in grazing waves. When the measuring window belongs to a wall with a smaller area, the grazing waves effect is reduced and leads to a decrease of the BDFI values. This phenomenon is represented by rooms C2 and C3 with smaller sections and lower BDFIs above the 630Hz third octave band. Standard devitations are also lower for these rooms. The boundary field is indeed more uniform here because of modes in the section with higher wave numbers.

This parametric study highlights the respective effects of the source position, the window position and the room dimensions on the BDFI and its standard deviation. From this short study we can conclude that the necessary conditions to reach a diffuse field are the following : stable mean BDFIs values around 1.8, and stable BDFI standard deviations below 0.5. However these necessary conditions

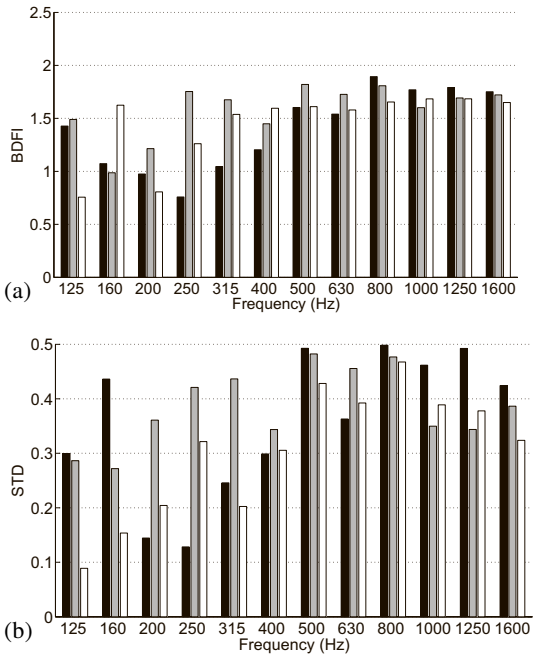


Figure 8. Room influence on the mean values and standard deviations of the calculated BDFIs over 400 patches - Configs. ■ C1a ■ C2 □ C3

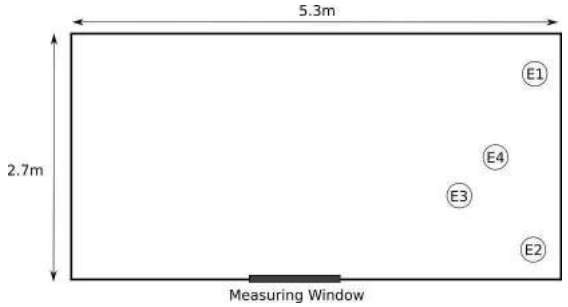


Figure 9. Source positions in the xy plane with $z_0 = 1.70\,\mathrm{m}$ and $L_z = 3\,\mathrm{m}$ - Measurement at UTC lab.

are not sufficient to insure a a diffuse field at boundaries. It is always important to look at the BDFI distribution in space to verify whether it is uniform and random or if it exhibits some patterns. Besides, in the analysis one must always keep in mind the size of the window compared to the acoustic wavelength and to the wall dimensions.

## 5. Experimental study

### 5.1. Experimental setup

Though the model gave a good understanding of particular phenomena at boundaries thanks to the Boundary Diffuse Field Index, a specific experimental study is still necessary to evaluate the relevance of this index in a practical situation. Measurements were thus made in two reverberant rooms in order to derive the corresponding Boundary Diffuse Field Indices (Equation 12) and standard deviations (Equation 13).

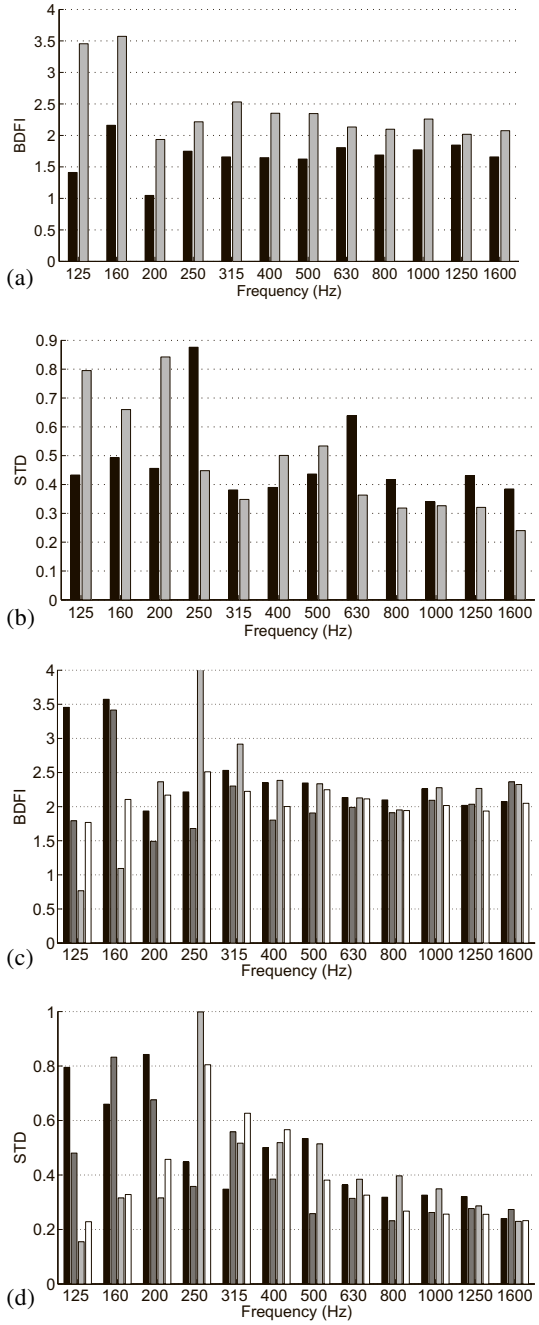


Figure 10. Comparison of measured and calculated BDFIs with the classical modal expansion for room configurations E1 (■ Calculated BDFI ■ Measured BDFI) – Comparison of measured BDFIs for several room configurations, ■ E1 ■ E2 ■ E3 □ E4.

A first series of measurements was conducted in the reverberant room of Université de technologie de Compiègne (France), and corresponds to configurations E1, E2, E3 and E4 detailed in Table I and recalled in Figure 9. Note that no diffusers were installed in the room. An omnipower omnidirectional sound source in a dodecahedral

configuration was used (Bruel & Kjaer 4292 type). For these measurements, a rotating microphone (1/2 inch microphone, Bruel & Kjaer 4190 type) was used to measure the spatially-averaged square room pressure, while another microphone (1/2 inch microphone, Bruel & Kjaer 4190 type) was translated using motorized axes in front of a wall surface discretized into 30x20 patches. This blocked pressure measurement was made at less than 1 cm from the wall and time signals were averaged over 10 seconds. The frequency analysis was made between 0 and 2000 Hz with a frequency step of 2.5 Hz.

Another series of measurements was conducted in the reverberant room of Groupe d'Acoustique de l'Université de Sherbrooke (Canada), and corresponds to configurations G1 and G2, detailed in Table I and presented in Figure 12. Several hanging and corner diffusers were installed in the room. For these measurements, a 1/2 inch rotating GRAS microphone was used to estimate the spatially-averaged square room pressure, while the spatial blocked pressure was now estimated using a microphone array. It was composed of 81 ($9 \times 9$) 1/4 inch microphones (Bruel & Kjaer 4958 type) spaced by 10 cm in both longitudinal and transversal directions, giving a square array of side length 0.8 m. Microphone capsules were positioned at a height 1 cm from the wall surface, and time signals were measured over 30 seconds using a sampling frequency $F_s = 8192$ Hz, and the frequency analysis was made between 0 and 2000 Hz with a frequency step of 2 Hz. An acoustic excitation was generated in the reverberant room using one low and mid frequencies speaker (JBL Eon) for a white noise input in the 50–2000 Hz frequency range.

For both measurements, local BDFIs were obtained using measured autospectra at the rotating microphone for the squared-room pressure $P_r^2$ and at the boundary microphones positions for the wall blocked pressures $|\langle P_b \rangle_i|^2$. The mean BDFI and the standard deviations were then calculated over the measurement surface from these local BDFIs. Note that preliminary measurements were made to verify that a microphone placed at 1 cm from the wall provided similar local BDFI results compared with those obtained using a flush mounted microphone on the wall up to the highest frequency of interest (*i.e.* 2 kHz).

### 5.2. Experimental BDFI results for configurations E1, E2, E3 and E4

Comparative results between calculated and measured BDFIs with the room configuration E1 are presented in the upper part of Figure 10. Experiments and theory both provide mean BDFI values between 1.5 and 2.5 above the 250Hz third octave band. Larger differences appear at low frequency. This is mainly due to differences in evaluating the room pressure. In theory it is averaged over the room volume, including the source and the intensification zones at boundaries, while in practice it is averaged with a moving probe. This is the main reason why the measured BDFIs are overestimated compared to the calculated BDFIs. The model assumes also an omnidirectional point source

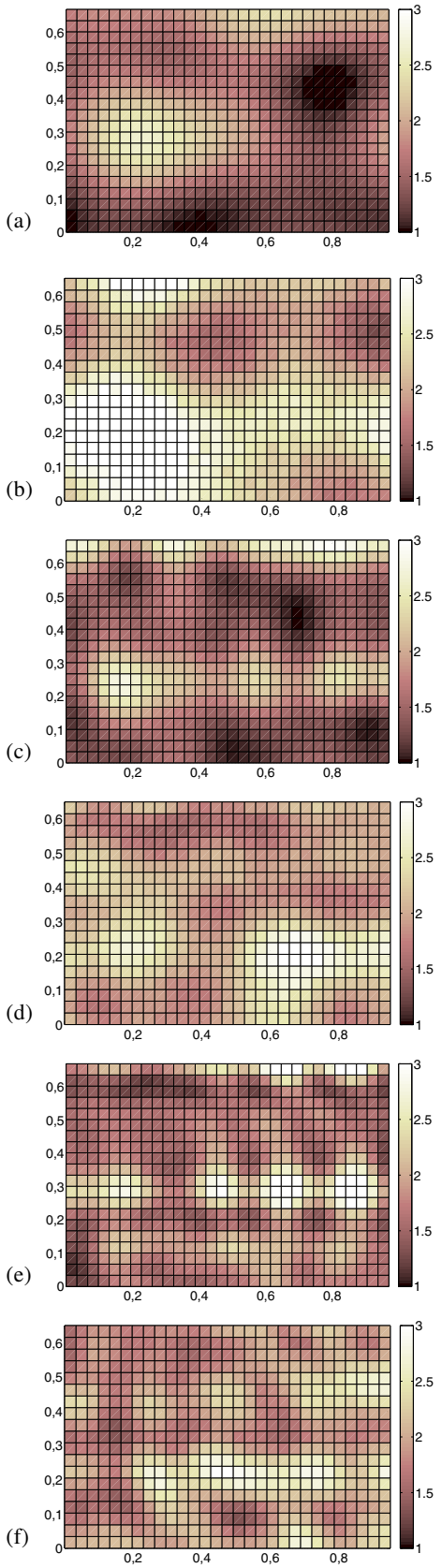


Figure 11. Comparison of calculated (a,c,e) and measured (b,d,f) xy spatial BDFI distributions on three third octave bands, (a,b): 400 Hz, (c,d): 800 Hz, (e,f): 1250 Hz. Room configuration E1.

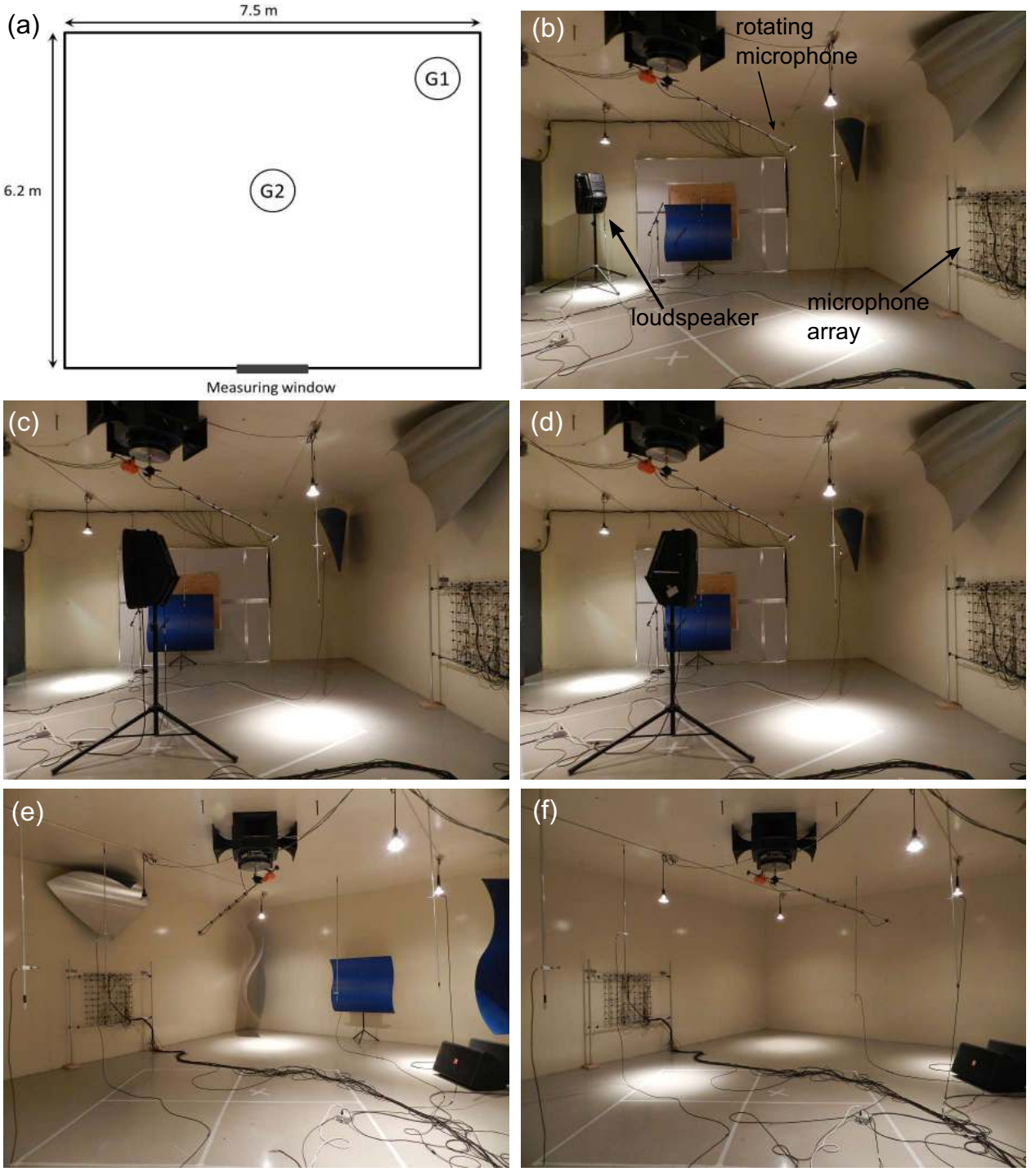


Figure 12. Measurement at GAUS lab: (a) Source positions in the xy plane with $z_0 = 1.5$m and $L_z = 3$m - (b) Picture of measurement with source position G1 - (c) Picture of measurement with source position G2 with the loudspeaker turned to the opposite wall from the measurement window - (d) Picture of measurement with source position G2 with the loudspeaker turned in front of the microphone array - (e) Viewpoint of the room from source position G1 with diffusers installed - (e) Viewpoint of the room from source position G1 with diffusers uninstalled.

whereas twelve loudspeakers in a dodecahedral configuration are used in practice. Finally the coupling with the panel mounted in the window is neglected and is assumed totally rigid in the model. On the other hand, standard deviations related to field homogeneity show a good agreement between theory and experiment. In this case, the pressure field is quite uniform with standard deviations around 0.35 above the 630 Hz third octave band.

Experimental and theoretical spatial BDFIs distributions obtained with configuration E1 are presented in Figure 11 for three third octave bands (400 Hz, 800 Hz and 1250 Hz). Calculated BDFIs are very similar to measured

ones. The same patterns are indeed observed in both cases. At low frequency a modal behaviour is well observed as expected, while at higher frequency, even above the cut off frequency, some more uniform patterns are visible. Hence, thanks to the BDFI mean values and standard deviations, different kinds of phenomena can be detected, even with a third octave analysis : the modal behaviour, a specific pressure pattern related to the acoustic wavelength, an important direct source contribution, or the effect of an intensification zone.

Finally the BDFIs and standard deviations measured with the four source positions E1-E2-E3-E4 are presented in the lower part of Figure 10. The classical cut off frequency at 630 Hz is clearly visible here with mean BDFIs stable around 2, and standard deviations stable around 0.3. However this cut off frequency is not sufficient to ensure a good diffuse field since the standard deviations values around 0.3 show some strong BDFI patterns (as seen previously in Figure 11 on the third octave centered at 1250 Hz).

### 5.3. Experimental BDFI results for configurations G1 and G2

Figure 12a schematically recalls the source positions and room dimensions for configuration G1 and G2. Pictures of the experiments are also given in Figures 12b-f. Two specific tests were made for the two considered source positions. For configuration G2 (when the source is installed at the center of the room), the loudspeaker was turned in front of the wall opposite to the microphone array, then turned in front of the microphone array to voluntarily increase the direct field contribution and the presence of correlated waves. Figures 12c,d show the two considered orientations of the sound source. The hanging diffusers placed in the room were also uninstalled for a measurement made with the source at position G1 to verify that their effect could be evaluated using the BDFI. Figures 12e,f show the room from the viewpoint of G1 source position with the diffusers present and uninstalled, respectively.

Figure 13 presents an experimental comparison between the measured mean room pressure and mean blocked pressure (at the center microphone array). As was shown in the case of numerical results in Figure 2, the mean blocked pressure exhibits very large variations compared to the mean room pressure, and a higher mean value.

The mean BDFIs obtained in configurations G1 and G2 (back-sided and front-sided speaker, from the measurement window view) and their spatial standard deviations are presented in the upper part of Figure 15. Configurations G1 and G2 (back-sided) provide very similar results above the 500 Hz third octave frequency band.

Also, the expected effect of turning the loudspeaker so that it faces the microphone array (*i.e.* increase of the direct field contribution and correlated waves) is very well illustrated with the G2 front-sided speaker case. The mean BDFI value now exceeds a value of 2 in nearly all the considered third octave bands compared to when the speaker was placed in front of the opposite wall.

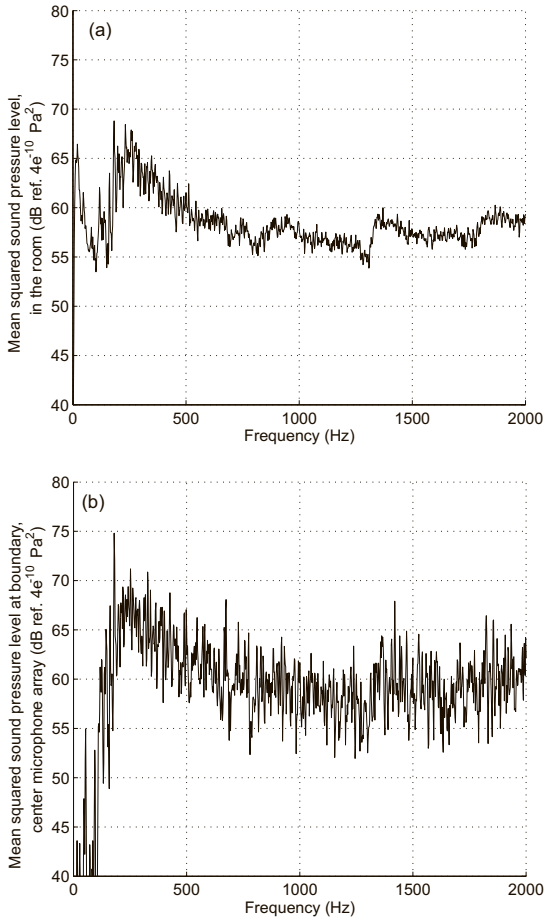


Figure 13. Source position G1 - Mean squared sound pressure level in the room measured with the rotating microphone (a), compared to the mean squared sound pressure level at a blocked pressure measurement point, here the center microphone of the array (b).

For the three considered cases and above the 315 Hz third octave band, standard deviations are stable and do not exceed a value of 0.4, and exhibit similar behavior compared to the standard deviation results previously obtained for the measurements at UTC.

Finally, lower part of Figure 15 presents the results obtained for the G1 source position, with and without hanging diffusers in the room.

The presence of the diffusers clearly smoothens the values of obtained BDFI around a value of 2 under the 630 Hz third octave band, and lowers the standard deviation which shows improvement of the sound field spatial homogeneity. This result, *i.e.* to expand the diffuse field at lower frequencies, is the expected result with such devices. However, these sound diffusers provides marginal improvement of the diffusivity at the room boundaries above the 630 Hz third octave band, as illustrated by similar BDFI and standard deviation values whether they were installed or not.

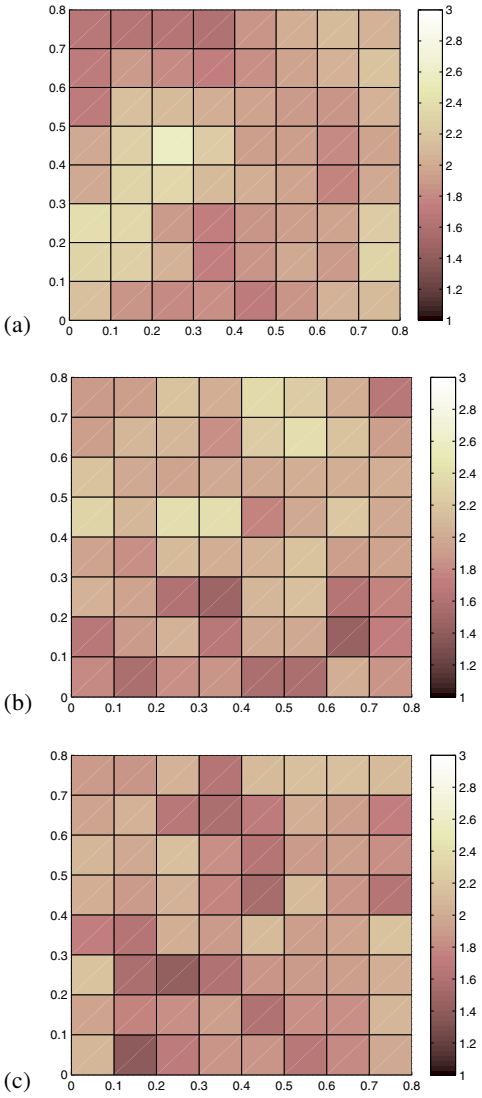


Figure 14. xy spatial BDFI distribution on third octave bands - Room configuration G1. (a) 400 Hz, (b) 800 Hz, (c) 1250 Hz.

## 6. Conclusion

Several parameters can change the diffusivity of a boundary sound field. The position of the measurement window on the wall have great importance due to intensification zones at the edges and corners of the room. Loudspeaker location in the room can also be a significant parameter especially if the direct source contribution becomes important, and the presence of diffusers have also a large influence on the boundary diffusivity at low frequency. The Boundary Diffuse Field Index presented in this article enables to study, either theoretically or experimentally, the global diffusivity of a boundary sound field due to all these phenomena. The BDFI distribution observed with a cartography at each frequency band, and characterized with a mean value and a standard deviation on the measurement window provides several interesting informations. Two particular aspects have hence been highlighted with this index: the isotropy of the field characterized by a limit incidence angle, and the correlation of incident waves.

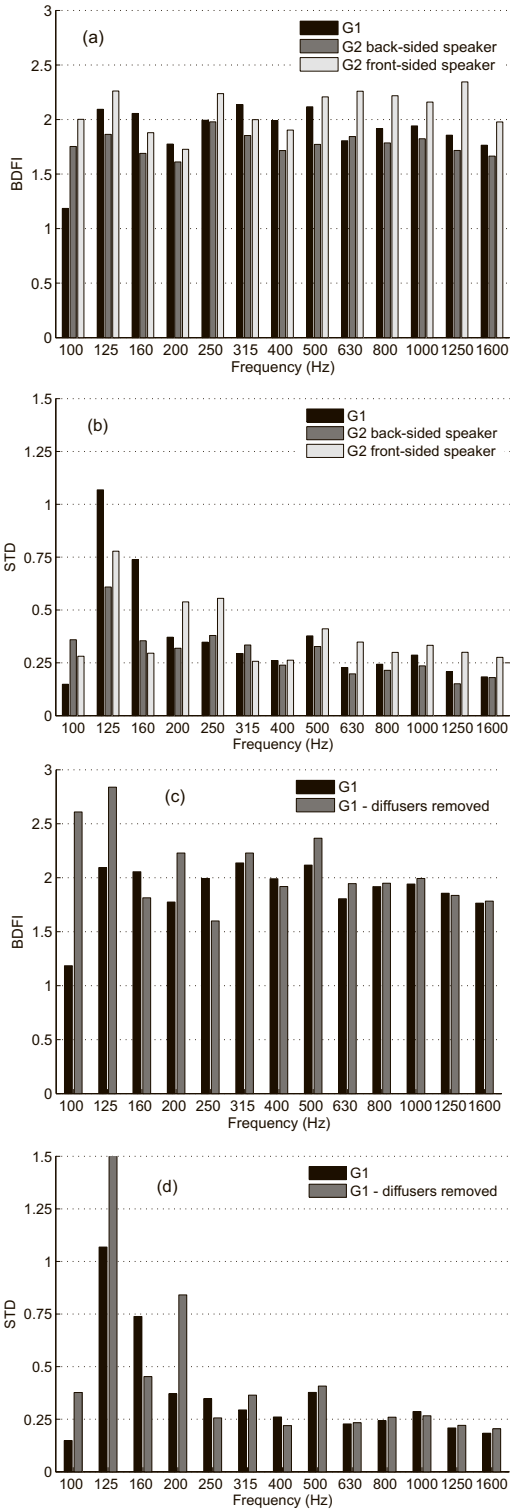


Figure 15. Measurement results on third octave bands for the source positions G1 and G2 : (a) Mean BDFI values and (b) BDFI Standard deviation - Results for the source position G1 with diffusers installed and uninstalled: (c) Mean BDFI values and (d) BDFI Standard deviation.

The interest of the BDFI is now to be employed as a diagnostic tool to characterize, to normalize, or to improve reverberant room facilities, knowing that a perfect room should show very low BDFIs standard deviations for homogeneity reasons of the boundary pressure field, and a mean BDFI close to a value of 2 to confirm a perfect isotropy of the boundary pressure field.

Further work involves relating the BDFI to transmission loss or sound absorption measurements.

## References


[1] ISO354-2003: Acoustics - measurement of sound absorption in a reverberation room. International Standard Organization, Geneva, Switzerland (2003).

[2] ASTM C423-09a: Standard test method for sound absorption and sound absorption coefficients by the reverberation room method. ASTM International, West Conshohocken, PA, USA (2009).

[3] ISO3741-2010: Acoustics - determination of sound power levels of noise sources using sound pressure - precision methods for reverberation rooms. International Standard Organization, Geneva, Switzerland (2010).

[4] ISO10140-2:2010: Acoustics - laboratory measurement of sound insulation of building elements - part 2: Measurement of airborne sound insulation. International Standard Organization, Geneva, Switzerland (2010).

[5] ISO15186-1:2000: Acoustics - measurement of sound insulation in buildings and of building elements using sound intensity - part 1: Laboratory measurements. International Standard Organization, Geneva, Switzerland (2000).

[6] ASTM E2249-02: Standard test method for laboratory measurement of airborne sound transmission loss of building partitions and elements using sound intensity. ASTM International, West Conshohocken, PA, USA (2002).

[7] ASTM E90-09: Standard test method for laboratory measurement of airborne sound transmission loss of building partitions and elements. ASTM International, West Conshohocken, PA, USA (2009).

[8] W. Sabine: Collected papers on acoustics. Harvard University Press, Cambridge , MA, USA, 1922, Ch. 1 - Reverberation, 3–68.

[9] M. Schroeder: The 'Schroeder frequency' revisited. J. Acoust. Soc. Am. **99** (1996) 3240–3241.

[10] C. Eyring: Reverberation time in 'dead' rooms. J. Acoust. Soc. Am. **1(2)** (1930) 217–241.

[11] C. Eyring: Reverberation time measurements in coupled rooms. J. Acoust. Soc. Am. **3** (1931) 181–206.

[12] G. Millington: A modified formula for reverberation. J. Acoust. Soc. Am. **4** (1932) 69–82.

[13] C. Balachandran: Random sound field in reverberation chambers. J. Acoust. Soc. Am. **31** (1959) 1319–1321.

[14] S. Dodd, P. Doak: Some aspects of the theory of diffusion and diffusers. J. Sound Vib. **16(1)** (1971) 89–98.

[15] C. Ebbing: Experimental evaluation of moving sound diffusers for reverberant rooms. J. Sound Vib. **16 (1)** (1971) 99–118.

[16] K. Boldlund: A study of diffusion in reverberation chambers provided with special devices. J. Sound Vib. **50(2)** (1977) 253–283.

[17] D. Bradley, M. Muller-Trapet, J. Adelgren, M. Vorlander: Effect of boundary diffusers in a reverberation chamber: Standardized diffuse field quantifiers. J. Acoust. Soc. Am. **135(4)** (2014) 1898–1906.

[18] D. Bradley, C. Diaz, E. Snow: Improved sound field reverberance and diffusivity in a reverberation chamber though implementation of resonant-diffusing wall panels. Acta Acust. United Ac. **101** (2015) 181–189.

[19] P. Fausti, R. Pompoli, R. Smith: An intercomparison of laboratory measurements of airborne sound insulation of lightweight plasterboard walls. Building Acoustics **6** (1999) 127–140.

[20] T. Bravo, S. Elliott: Variability of low frequency sound transmission measurements. J. Acoust. Soc. Am. **115(6)** (2004) 2986–2997.

[21] R. Jones: Intercomparisons of laboratory determinations of airborne sound transmission loss. J. Acoust. Soc. Am. **66** (1979) 148–164.

[22] A. Warnock, M. Vorlander: Inter-laboratory comparison of low frequency sound transmission - finite element studies. Proceedings of Internoise, Leuven, Belgium, 1993, 929–932.

[23] M. Vorlander, A. Warnock: Inter-laboratory comparison of low frequency sound transmission - conventional and intensity measurements. Proceedings of Internoise, Leuven, Belgium, 1993, 933–936.

[24] A. Dijckmans, C. Vermeir: Numerical investigation of the repeatability and reproducibility of laboratory sound insulation measurements. Acta Acust. United Ac. **99** (2013) 421–432.

[25] C. Kosten: International comparison measurements in the reverberation room. Acustica **10** (1960) 400–411.

[26] G. Benedetto, E. Brosio, T. Spagnolo: The effect of stationary diffusers in the measurement of sound absorption coefficients in a reverberant room : an experimental study. Appl. Acoust. **14 (1)** (1981) 49–63.

[27] J. Davy, W. Davern, P. Dubout: Qualification of room diffusion for absorption measurements. Appl. Acoust. **28** (1989) 177–185.

[28] R. Halliwell: Inter-laboratory variability of sound absorption measurement. J. Acoust. Soc. Am. **73(3)** (1983) 880–886.

[29] A. Nash: On the reproducibility of measuring random incidence sound absorption. Proceedings of Internoise 2012, 19-22 August, New-York City, USA, 2012.

[30] P. Dammig: Model investigations into sound fields in reverberation rooms. Acta Acust. United Ac. **75** (1991) 105–120.

[31] A. Toyoda, S. Sakamoto, H. Tachibana: Effects of room shape and diffusing treatment on the measurement of sound absorption coefficient in a reverberation room. Acoust. Sci. and Tech. **25** (2004) 255–266.

[32] T. Schultz: Diffusion in reverberant rooms. J. Sound Vib. **16(1)** (1971) 17–28.

[33] N. Spring, K. Randall: The measurement of sound diffusion index in small rooms. Tech. Rept. BBC research department, Report No 1969/16, 1969.

[34] J. Bassett, D. Spargo, D. Cabrera: Using an ambisonic microphone for measurement of the diffuse state in a reverberant room. Proceedings of 20th International Congress on Acoustics, ICA 2010, 23-27 August, Sydney, Australia, 2010.

[35] B. Gover, J. Ryan, M. Stinson: Microphone array measurement system for analysis of directional and spatial variations of sound fields. J. Acoust. Soc. Am. **112** (2002) 1980–1991.

[36] R. Cook, R. Waterhouse, D. Berendt, S. Edelman, M. Thompson Jr.: Measurement of correlation coefficients reverberant sound fields. J. Acoust. Soc. Am. **27** (1955) 1072–1077.

[37] B. Rafaely: Spatial-temporal correlation of a diffuse sound field. J. Acoust. Soc. Am. **107** (2000) 3254–3258.

[38] R. Waterhouse: Statistical properties of reverberant sound fields. J. Acoust. Soc. Am. **43** (1968) 1436–1444.

[39] R. Waterhouse: Noise measurement in reverberant rooms. J. Acoust. Soc. Am. **54** (1973) 931–934.

[40] C. Morrow: Point-to-point correlation of sound pressures in reverberation chambers. J. Sound Vib. **16(1)** (1971) 29–42.

[41] I. Chun, B. Rafaely, P. Joseph: Experimental investigation of spatial correlation in broadband reverberant sound fields. J. Acoust. Soc. Am. **113(4)** (2003) 1995–1998.

[42] B. Arguillat, D. Ricot, C. Bailly, G. Robert: Measured wavenumber: Frequency spectrum associated with acoustic and aerodynamic wall pressure fluctuations. J. Acoust. Soc. Am. **128(4)** (2010) 1647–1655.

[43] O. Robin, N. Atalla, H. Osman: Investigating the sound field characteristics in a reverberant room using 2D cross-spectral density measurement. Proceedings of the NoiseCon14 Congress, Fort Lauderdale, FL, USA, September 8-10, 2014.

[44] K. Boldlund: A new quantity for comparative measurements concerning the diffusion of stationary sound fields. J. Sound Vib. **44(2)** (1976) 191–207.

[45] J. Coyette, G. Lielens, M. Robb, P. Neple: An efficient method for evaluating diffuse field joint acceptance functions for cylindrical and truncated conical geometries. J. Acoust. Soc. Am. **117** (2005) 1009–1019.

[46] S. Elliott, C. Maury, P. Gardonio: The synthesis of spatially correlated random pressure fields. J. Acoust. Soc. Am. **117** (2005) 1186–1201.

[47] O. Robin, A. Berry, S. Moreau: Experimental vibroacoustic testing of plane panels using synthesized random pressure fields. J. Acoust. Soc. Am. **135(6)** (2014) 3434–3445.

[48] H. Nelisse, J. Nicolas: Characterization of a diffuse field in a reverberant room. J. Acoust. Soc. Am. **101** (1997) 3517–3524.

[49] F. Jacobsen, T. Roisin: The coherence of reverberant sound fields. J. Acoust. Soc. Am. **108** (2000) 204–210.

[50] M. Kuster: Spatial correlation and coherence in reverberant acoustic fields: Extension to microphones with arbitrary first-order directivity. J. Acoust. Soc. Am. **123(1)** (2008) 154–162.

[51] R. Waterhouse: Interference patterns in reverberant sound fields. J. Acoust. Soc. Am. **27** (1955) 247–258.

[52] K. Lynch, P. Bauch, S. Hambric, A. Barnard: A proposed correction for incident sound intensity distribution for diffuse field panel excitation and transmission loss simulations. Proceedings of Noise-Con 2014, Fort Lauderdale, Florida, USA, September 8-10, 2014.

[53] L. Franzoni, D. Labrozzi: A study of damping effects on spatial distribution and level of reverberant sound in a rectangular acoustic cavity. J. Acoust. Soc. Am. **106** (1999) 802–815.

[54] R. Waterhouse, R. Cook: Diffuse sound fields: Eigenmode and free-wave models. J. Acoust. Soc. Am. **59** (1976) 576–581.

[55] J.-D. Chazot, J.-L. Guyader: Prediction of transmission loss of double panels with a patch-mobility method. J. Acoust. Soc. Am. **121** (2007) 267–278.

[56] J.-D. Chazot, J.-L. Guyader: Transmission loss of double panels filled with porogranular materials. J. Acoust. Soc. Am. **126** (2009) 3040–3048.